Magnetoelectricity in multiferroic particulate composites with arbitrary crystallographic orientation

2012 Smart Mater. Struct. 21 105038

(http://iopscience.iop.org/0964-1726/21/10/105038)

Smart Mater. Struct. **21** (2012) 105038 (10pp) doi:10.1088/0964-1726/21/10/105038

Magnetoelectricity in multiferroic particulate composites with arbitrary crystallographic orientation

Hsin-Yi Kuo and You-Min Kuo

Department of Civil Engineering, National Chiao Tung University, Hsinchu 30010, Taiwan

E-mail: hykuo@mail.nctu.edu.tw

Received 29 May 2012, in final form 18 July 2012
Published 7 September 2012
Online at stacks.iop.org/SMS/21/105038

Abstract
This paper studies the magnetoelectricity (ME) of a spherical particulate composite made of piezoelectric and piezomagnetic phases. The effects of crystallographic orientations and the volume fraction of inclusion are investigated by a micromechanical approach. The solutions are in good agreement with predictions by finite element analysis. Based on this micromechanical method, we show that, for the $CoFe_2O_4$–$LiNbO_3$ particulate composite, the effective ME voltage coefficient can be enhanced at the optimal orientation as compared to those at normal cut orientation. Further, we observe that the ME coupling is sensitive to the piezoelectric constant e_{15}. The optimal orientation of the ME voltage coefficient is near that of the piezoelectric constant e_{15}.

(Some figures may appear in colour only in the online journal)

1. Introduction

Multiferroic materials, which show simultaneously two or more types of ferroelectric, ferromagnetic or ferroelastic ordering, have been the focus of research due to their varieties of microstructural phenomena and overall properties (Wang *et al* 2003, Lottermoser *et al* 2004, Ramesh and Spaldin 2007, Catalan and Scott 2009). This makes multiferroics particularly appealing and promising for practical device applications, ranging from four-state memory cells (Vopsaroiu *et al* 2007) and large-area sensitive detection of magnetic fields (Fiebig 2005) to energy harvesting (Bayrashev *et al* 2004). However, the magnetoelectric (ME) effect in single-phase materials is rather weak or cannot be observed at room temperature (Astrov 1960, Rado and Folen 1961). Composite materials made of piezoelectric and magnetostrictive/piezomagnetic phases, on the other hand, offer an alternative option for improvement of the ME coupling, as explained in recent reviews by Eerenstein *et al* (2006), Nan *et al* (2008) and Bichurin *et al* (2010). Basically it was suggested that the ME effect could be generated artificially as a product property,

$$\text{magnetoelectric effect} = \frac{\text{electric}}{\text{mechanical}} \times \frac{\text{mechanical}}{\text{magnetic}}.$$

This states that an applied magnetic field creates a strain in the piezomagnetic/magnetostrictive material which in turn creates a strain in the piezoelectric material, resulting in an electric polarization.

Motivated by the numerous practical applications and the indirect coupling through strain, a variety of theoretical studies have been proposed to predict the effective ME moduli of the multiferroic composite. Predictions of the macroscopic properties of ME composites have been obtained by, for example, the Mori–Tanaka approach (Huang and Kuo 1997, Li and Dunn 1998a), the Green's function and perturbation theory (Nan 1994), the homogenization technique (Aboudi 2001, Camacho-Montes *et al* 2009), the variational asymptotic method (Tang and Yu 2008, 2009) or finite element analysis (Liu *et al* 2004, Lee *et al* 2005). Further, exact relations among the moduli in an ME composite with cylindrical geometry were derived by Benveniste (1995). The local field distribution is also available for periodic arrays of circular/elliptic fibrous ME composites (Kuo 2011, Kuo and Pan 2011) and laminates (Srinivasan *et al* 2001, Bichurin *et al* 2003).

Recently, experiments by Yang *et al* (2006) and Wang *et al* (2008) showed that single crystals are attractive and

the effective ME coefficient of a laminate is sensitive to the crystallographic orientation of the material. In fact, the effect of crystal anisotropy on the ME coupling has been analyzed to certain extent. For example, Li and Dunn (1998b) used Eshelby's equivalent inclusion approach to study the fields in and around inclusions/inhomogeneities in anisotropic solids exhibiting full coupled field behavior. Later, Li (2000) proposed a numerical algorithm to calculate the ME Eshelby tensor for an ellipsoidal inclusion with arbitrary material symmetry. Srinivas *et al* (2006) developed a mean field Mori–Tanaka model to calculate the ME coupling of matrix-based multiferroic composites, emphasizing the effects of shape and orientation distribution of second-phase particles. Further, theoretical frameworks were proposed to optimize the effective ME response of a piezoelectric–magnetostrictive bilayer (Kuo *et al* 2010), multilayers (Kim 2011) and an ME fibrous composite (Kuo and Wang 2012). The basic concept of these works is that the induced electric field can be increased if the poling direction/magnetic axis and volume fraction of the constituents are carefully chosen. Following this idea, in this work we investigate the crystallographical orientation dependent ME voltage coefficient of a multiferroic composite with spherical particles.

This paper is organized as follows. First the basic equations and transformation rules regarding the magneto-electroelasticity are introduced in section 2. In section 3, we define the effective properties of the composite. We present a micromechanical model for estimating the effective moduli of the multiferroic composite in section 3.1, while the finite element method is proposed in section 3.2. Both methodologies are illustrated in section 4 using composites of cobalt ferrite ($CoFe_2O_4$) and lithium niobate ($LiNbO_3$) or barium titanate ($BaTiO_3$). We show that the optimal orientations can be non-trivial and that the enhancement is many-fold over the normal orientations. Finally, we observe that the ME coupling is sensitive to the piezoelectric constant e_{15}.

2. Formulation

Consider a spherical particulate composite made of piezoelectric and piezomagnetic materials. The general constitutive laws for the rth phase are described by the following equations (Alshits *et al* 1992):

$$\begin{aligned}\boldsymbol{\sigma}^{(r)} &= \mathbf{C}^{(r)}\boldsymbol{\varepsilon}^{(r)} - \mathbf{e}^{\mathrm{t}(r)}\mathbf{E}^{(r)} - \mathbf{q}^{\mathrm{t}(r)}\mathbf{H}^{(r)},\\ \mathbf{D}^{(r)} &= \mathbf{e}^{(r)}\boldsymbol{\varepsilon}^{(r)} + \boldsymbol{\kappa}^{(r)}\mathbf{E}^{(r)} + \boldsymbol{\lambda}^{\mathrm{t}(r)}\mathbf{H}^{(r)},\\ \mathbf{B}^{(r)} &= \mathbf{q}^{(r)}\boldsymbol{\varepsilon}^{(r)} + \boldsymbol{\lambda}^{(r)}\mathbf{E}^{(r)} + \boldsymbol{\mu}^{(r)}\mathbf{H}^{(r)},\end{aligned} \tag{2.1}$$

where $\boldsymbol{\sigma}$, $\mathbf{D}$, $\mathbf{B}$, $\boldsymbol{\varepsilon}$, $\mathbf{E}$ and $\mathbf{H}$ are the stress, electric displacement, magnetic flux, strain, electric field and magnetic field respectively. $\mathbf{C}$ is the fourth-order tensor of elastic moduli, $\mathbf{e}$ and $\mathbf{q}$ are the third-order tensors of piezoelectric and piezomagnetic constants, $\boldsymbol{\kappa}$, $\boldsymbol{\mu}$ and $\boldsymbol{\lambda}$ are the second-order tensors of the dielectric permittivity, magnetic permeability and magnetoelectric coefficient. The superscript t is used to denote the matrix transpose. The symmetry conditions satisfied by the moduli are given by Nye (1985).

The strain $\boldsymbol{\varepsilon}$, electric field $\mathbf{E}$ and magnetic field $\mathbf{H}$ are respectively defined by the displacement $\mathbf{u}$, electric potential φ and magnetic potential ψ via

$$\boldsymbol{\varepsilon} = \tfrac{1}{2}(\nabla\mathbf{u} + (\nabla\mathbf{u})^{\mathrm{t}}), \qquad \mathbf{E} = -\nabla\varphi, \qquad \mathbf{H} = -\nabla\psi. \tag{2.2}$$

On the other hand, when no free charge or body force is assumed to exist, the stress, electric displacement and magnetic intensity satisfy the following equilibrium equations:

$$\nabla\cdot\boldsymbol{\sigma} = \mathbf{0}, \qquad \nabla\cdot\mathbf{D} = 0, \qquad \nabla\cdot\mathbf{B} = 0, \tag{2.3}$$

along with the analogous interfacial conditions

$$\begin{aligned}[\![\boldsymbol{\sigma}\mathbf{n}]\!] = \mathbf{0}, \qquad [\![\mathbf{D}\cdot\mathbf{n}]\!] = 0, \qquad [\![\mathbf{B}\cdot\mathbf{n}]\!] = 0,\\ [\![\mathbf{u}]\!] = \mathbf{0}, \qquad [\![\varphi]\!] = 0, \qquad [\![\psi]\!] = 0,\end{aligned} \tag{2.4}$$

where $[\![\cdot]\!]$ denotes the jump in some quantity across the interface, and $\mathbf{n}$ is the unit outward normal to the interface.

The constitutive laws (2.1), strain–displacement (2.2) and equilibrium equations (2.3) can be rewritten in a more compact form as follows (Alshits *et al* 1992):

$$\Sigma_{iJ} = L_{iJMn}Z_{Mn}, \qquad Z_{Mn} = U_{M,n}, \qquad \Sigma_{iJ,i} = 0, \tag{2.5}$$

where

$$\Sigma_{iJ} = \begin{cases}\sigma_{ij}, & J = 1\text{–}3,\\ D_i, & J = 4,\\ B_i, & J = 5,\end{cases}$$

$$Z_{Mn} = \begin{cases}\varepsilon_{mn}, & M = 1\text{–}3,\\ -E_n, & M = 4,\\ -H_n, & M = 5,\end{cases} \tag{2.6}$$

$$U_M = \begin{cases}u_m, & M = 1\text{–}3,\\ \varphi, & M = 4,\\ \psi, & M = 5.\end{cases}$$

The magnetoelectroelastic moduli are expressed as

$$L_{iJMn} = \begin{cases}C_{ijmn}, & J, M = 1\text{–}3,\\ e_{ijn}, & M = 4, J = 1\text{–}3,\\ q_{ijn}, & M = 5, J = 1\text{–}3,\\ e_{imn}, & J = 4, M = 1\text{–}3,\\ -\kappa_{in}, & J = 4, M = 4,\\ -\lambda_{in}, & J = 4, M = 5,\\ q_{imn}, & J = 5, M = 1\text{–}3,\\ -\lambda_{in}, & J = 5, M = 4,\\ -\mu_{in}, & J = 5, M = 5,\end{cases} \tag{2.7}$$

where the upper case subscripts range from 1 to 5 and the lower case subscripts range from 1 to 3. Repeated upper case subscripts are summed from 1 to 5.

The equations above refer the material properties to the composite frame $x_1x_2x_3$. However, the material properties are commonly described in the crystallographic frame $x_1'x_2'x_3'$

and we need to transform them to the composite frame. For this purpose, the L_{iJMn} can be obtained from their principal values using tensor transformation rules for second-, third- and fourth-order tensors,

$$\begin{aligned} \kappa_{ij} &= a_{im}a_{jn}\kappa'_{mn}, & \mu_{ij} &= a_{im}a_{jn}\mu'_{mn}, \\ e_{ijk} &= a_{im}a_{jn}a_{ko}e'_{mno}, & q_{ijk} &= a_{im}a_{jn}a_{ko}q'_{mno}, \\ C_{ijkl} &= a_{im}a_{jn}a_{ko}a_{lp}C'_{mnop}, \end{aligned} \tag{2.8}$$

where the transformation matrix a_{ij} is given by Arfken and Weber (2001) as

$$\begin{pmatrix} a_{11} & a_{12} & a_{13} \\ a_{21} & a_{22} & a_{23} \\ a_{31} & a_{32} & a_{33} \end{pmatrix} = \begin{pmatrix} \cos\gamma\cos\beta\cos\alpha - \sin\gamma\sin\alpha & \cos\gamma\cos\beta\sin\alpha + \sin\gamma\cos\alpha & -\cos\gamma\sin\beta \\ -\sin\gamma\cos\beta\cos\alpha - \cos\gamma\sin\alpha & -\sin\gamma\cos\beta\sin\alpha + \cos\gamma\cos\alpha & \sin\gamma\sin\beta \\ \sin\beta\cos\alpha & \sin\beta\sin\alpha & \cos\beta \end{pmatrix}. \tag{2.9}$$

Here (α, β, γ) are the three Euler angles, and the primed quantities $(\kappa'_{ij}, \mu'_{ij}, e'_{ijk}, q'_{ijk}, C'_{ijkl})$ denote the material properties referred to the crystallographic frame.

3. Effective moduli

In this study, we are interested in the macroscopic behavior of the heterogeneous material. We first recall the basic definition of the effective magnetoelectroelastic parameter $\mathbf{L}^*$,

$$\langle \mathbf{\Sigma} \rangle = \mathbf{L}^* \langle \mathbf{Z} \rangle , \tag{3.1}$$

where $\langle\cdot\rangle = 1/V \int_V (\cdot)\, \mathrm{d}V$ denotes the volume average over the representative volume element (unit cell in the case of periodic composites). Specifically, an important figure of merit of the magnetoelectric composite is the ME voltage coefficient, $\alpha^*_{E,ij}$, which relates the overall electric field generated in the composite with the applied magnetic field. It combines the ME constant and dielectric coefficient, and is defined by

$$\alpha^*_{E,ij} = \lambda^*_{ij}/\kappa^*_{ij}, \qquad \text{no summation.} \tag{3.2}$$

Note that the magnetoelectric coefficient, λ^*_{ij}, is non-zero for the ME composite even though this coefficient is zero in each phase, i.e., $\lambda_{ij} = 0$.

3.1. Micromechanical approach

In order to determine the effective magnetoelectroelastic moduli defined in (3.1), we first turn to the micromechanical model for this purpose. Due to the linearity, the generalized strain in the inclusion for a two-phase composite is (Srinivas *et al* 2006)

$$\mathbf{Z} = \mathbf{A} \langle \mathbf{Z} \rangle , \tag{3.3}$$

where $\mathbf{A}$ is the generalized strain concentration tensor of the inclusion, satisfying $\langle \mathbf{A} \rangle = \mathbf{I}$. Here $\mathbf{I}$ is the fourth-order identity tensor. Substituting equation (3.3) into (3.1), together with the average generalized stress and strain theorems, the effective moduli thus can be determined for a two-phase composite as

$$\mathbf{L}^* = \mathbf{L}^{(m)} + f\left(\mathbf{L}^{(i)} - \mathbf{L}^{(m)}\right)\mathbf{A}. \tag{3.4}$$

Here f is the volume fraction of the inclusion, and the superscripts m and i denote the matrix and inclusion, respectively. The concentration tensor $\mathbf{A}$ can be determined by a variety of models. Among them, the Mori–Tanaka approach is very powerful. The essence of the Mori–Tanaka approach is that the averaging field in the rth phase of the composite is equivalent to the field in a single particle embedded in an infinite medium (Srinivas *et al* 2006). Using this approach, the concentration factor can be determined as

$$\mathbf{A} = \mathbf{A}^{\mathrm{dil}}\left[(1-f)\,\mathbf{I} + f\mathbf{A}^{\mathrm{dil}}\right]^{-1}, \tag{3.5}$$

with the dilute concentration tensor $\mathbf{A}^{\mathrm{dil}}$ given by

$$\mathbf{A}^{\mathrm{dil}} = \left[\mathbf{I} + \mathbf{S}(\mathbf{L}^{(m)})^{-1}\left(\mathbf{L}^{(i)} - \mathbf{L}^{(m)}\right)\right]^{-1}. \tag{3.6}$$

Here $\mathbf{S}$ is the magnetoelectroelastic Eshelby tensor, which is a function of the magnetoelectroelastic moduli of the matrix and the shape and orientation of the inclusion, and is described by Li and Dunn (1998b)

$$S_{MnAb} = \frac{1}{8\pi} L_{iJAb} \times \begin{cases} \displaystyle\int_{-1}^{1}\int_{0}^{2\pi} \left[G_{mJin}(\mathbf{z}) + G_{nJim}(\mathbf{z})\right] \mathrm{d}\theta\, \mathrm{d}\xi_3, \\ \qquad M = 1, 2, 3, \\ \displaystyle 2\int_{-1}^{1}\int_{0}^{2\pi} G_{4Jin}(\mathbf{z})\, \mathrm{d}\theta\, \mathrm{d}\xi_3, \qquad M = 4, \\ \displaystyle 2\int_{-1}^{1}\int_{0}^{2\pi} G_{5Jin}(\mathbf{z})\, \mathrm{d}\theta\, \mathrm{d}\xi_3, \qquad M = 5. \end{cases} \tag{3.7}$$

In the above equation, $z_i = \xi_i/a_i$ (no summation on i), a_i is the semi-axis of size and ξ_1 and ξ_2 can be expressed in terms of ξ_3 and θ by $\xi_1 = \sqrt{1-\xi_3^2}\cos\theta$ and $\xi_2 = \sqrt{1-\xi_3^2}\sin\theta$. In addition, $G_{MJin} = z_i z_n K^{-1}_{MJ}(z)$, where K^{-1}_{MJ} is the inverse of $K_{JR} = z_i z_n L_{iJRn}$. Li and Dunn (1998a) have obtained the closed-form expressions of the magnetoelectroelastic Eshelby tensors for fibrous or penny shaped particles in a transversely isotropic medium. However, for piezoelectric and piezomagnetic materials with spherical shapes or with arbitrary poling direction/magnetic axes as discussed in this work, we should resort to the Gauss quadrature numerical method to calculate S_{MnAb}. The integral (3.7) then is approximated by the weighted sum of function values at certain integration points (Li 2000).

3.2. Finite element method

The analysis carried out in the previous subsection is for an arbitrary system with a number of particles. Here, we

Table 1. Material parameters of $BaTiO_3$ (Pan 2001), $CoFe_2O_4$ (Pan 2001), $LiNbO_3$ (Weis and Gaylord 1985).

Property	$CoFe_2O_4$	$LiNbO_3$	$BaTiO_3$
C_{11} (GPa)	286	203	166
C_{12} (GPa)	173	53	77
C_{13} (GPa)	170.5	75	78
C_{33} (GPa)	269.5	245	162
C_{44} (GPa)	45.3	60	43
C_{66} (GPa)	56.5	75	44.5
C_{14} (GPa)	0	9	0
C_{56} (GPa)	0	9	0
κ_{11} (nC^2 N^{-1} m^{-2})	0.08	0.39	11.2
κ_{33} (nC^2 N^{-1} m^{-2})	0.093	0.26	12.6
μ_{11} (μN s^2 C^{-2})	590	5	5
μ_{33} (μN s^2 C^{-2})	157	10	10
e_{15} (C m^{-2})	0	3.7	11.6
e_{16} (C m^{-2})	0	−2.5	0
e_{21} (C m^{-2})	0	−2.5	0
e_{31} (C m^{-2})	0	0.2	−4.4
e_{33} (C m^{-2})	0	1.3	18.6
q_{15} (N A^{-1} m^{-1})	550	0	0
q_{31} (N A^{-1} m^{-1})	580.3	0	0
q_{33} (N A^{-1} m^{-1})	699.7	0	0

introduce the finite element analysis to study the case of periodic arrays of spheres which is used for comparison with the above micromechanical approach. We first choose an appropriate representative volume element (RVE), a periodic unit cell. There are seven crystal systems to pack spheres in a regular array in space (see Kittel (2005), for instance). Here we concentrate on the cubic system, specifically the face-centered cubic lattice.

The basic equations are the same as described in section 2. Further, due to the periodicity in the composite structure, the displacement u_i, the electric potential φ and the magnetic potential ψ in any point of the unit cell can be expressed in terms of those at an equivalent point in another RVE such that the periodic boundary conditions

$$\begin{aligned} U_M(d, x_2, x_3) &= U_M(-d, x_2, x_3) + \langle U_{M,1} \rangle 2d, \\ U_M(x_1, d, x_3) &= U_M(x_1, -d, x_3) + \langle U_{M,2} \rangle 2d, \\ U_M(x_1, x_2, d) &= U_M(x_1, x_2, -d) + \langle U_{M,3} \rangle 2d \end{aligned} \tag{3.8}$$

are satisfied for the cubic lattice. Here U_M is as defined in (2.6) and $2d$ is the length of the unit cell. The comma in the subscript denotes the partial derivative.

To determine the effective properties of the above periodic multiferroic composite, the strain ε_{ij}, electric field E_i and magnetic field states H_i are applied individually to the unit cell. For example, by applying a constant uniaxial electric field $\langle \varphi_{,1} \rangle = \langle -E_1 \rangle$ with all of the other averaged terms zero, one can construct one of the independent boundary value problems. By applying the twelve independent states to the RVE, each effective coefficient can be determined by (3.1). We perform the finite element analysis using the COMSOL Multiphysics software.

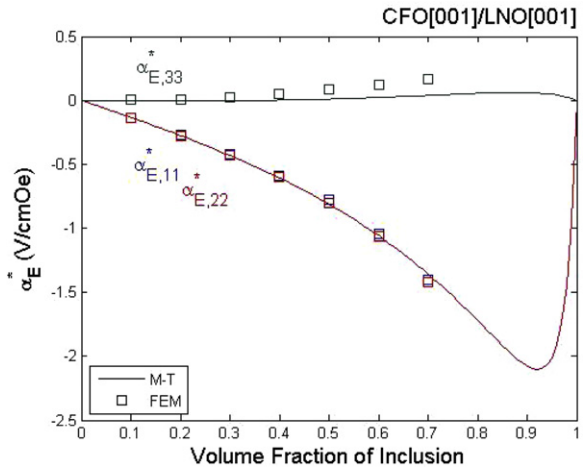

Figure 1. The ME voltage coefficients of the CFO particles in an LNO matrix in the normal direction versus the particle volume fraction.

4. Numerical results and discussion

In order to have a better understanding of the theoretical results above, we consider a variety of systems of interest. For the piezoelectric (PE) material, we consider the lead-free ferroelectric $LiNbO_3$ (LNO) (3 m symmetry) as well as the widely used $BaTiO_3$ (BTO) ceramic (6 mm symmetry). For the piezomagnetic (PM) material we consider $CoFe_2O_4$ (CFO) (6 mm symmetry) which has been studied by other researchers. We consider face-centered cubic arrays in finite element analysis. The independent material constants of these constituents are given in table 1 in Voigt notation, where the poling direction/magnetic axis is along the x_3-direction.

4.1. Piezomagnetic particles in a piezoelectric matrix

We begin with the case of PM particles in a PE matrix. We first consider lithium niobate as the PE phase. To check the correctness of our model, we first perform a numerical computation for CFO particles in an LNO matrix with magnetic axis/poling direction along the x_3-axis. Figure 1 shows the ME voltage coefficients for this composite. The finite element analysis is estimated for discrete volume fractions and stops around $f = \sqrt{2}\pi/6 = 0.740$ when the inclusions touch for the face-centered cubic lattice. The prediction of the Mori–Tanaka approach is in good agreement with the result of the finite element analysis. The maximum ME voltage coefficients $\alpha^*_{E,11}$ and $\alpha^*_{E,22}$ are -2.1023 V cm^{-1} Oe^{-1} at a volume fraction of $f = 0.92$, while the maximum $\alpha^*_{E,33} = 0.0619$ V cm^{-1} Oe^{-1} at a volume fraction of $f = 0.88$.

We now turn to investigation of the effect of the crystallographic orientation angle of this composite. For each orientation, we follow the procedure developed in the previous section to obtain the ME voltage coefficient. The reference volume fraction is chosen as $f = 0.92$ since this happens be optimal at the normal cut. The poling direction/magnetic axes of both constituents are arbitrary. Note that due to the

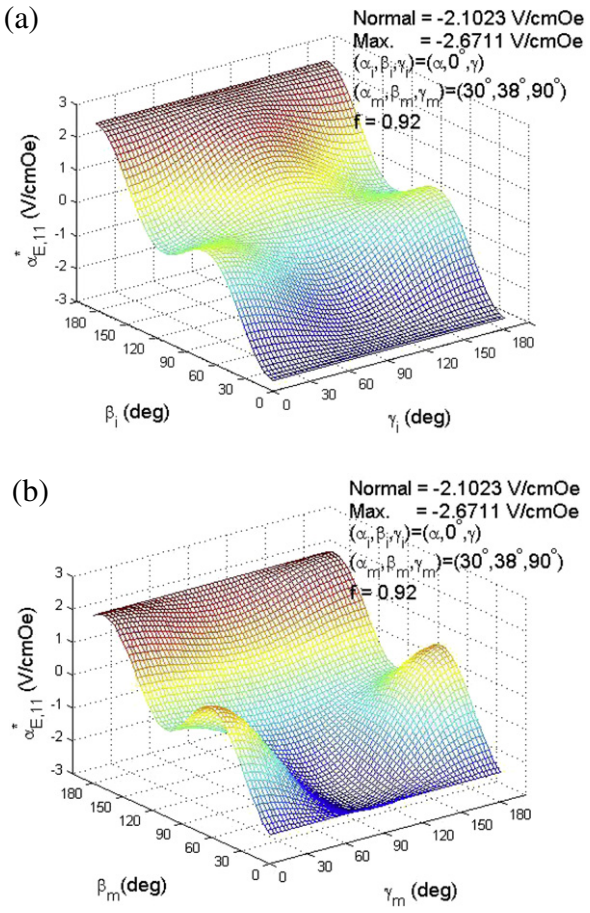

Figure 2. The ME voltage coefficient $\alpha^*_{E,11}$ of the CFO particles in an LNO matrix for various orientations of the CFO and LNO. The subscripts i and m denote the inclusion and matrix, respectively. Note that this coefficient is independent of the Euler angle α_i.

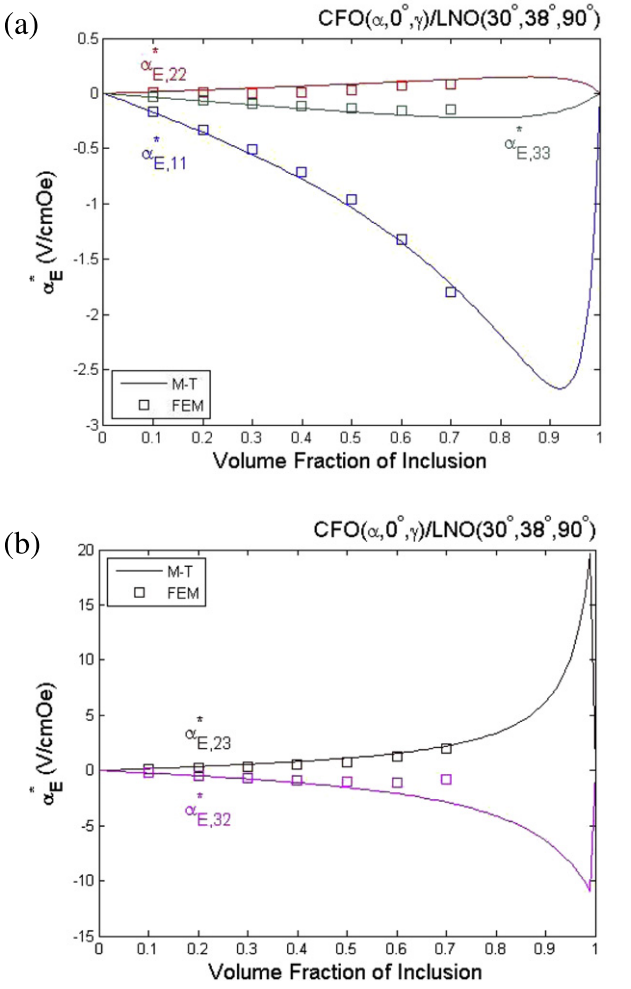

Figure 3. The optimal ME voltage coefficients of the CFO particles in an LNO matrix for various particle volume fractions. (a) Diagonal ME voltage coefficients $\alpha^*_{E,11}$, $\alpha^*_{E,22}$ and $\alpha^*_{E,33}$. (b) Off-diagonal ME voltage coefficients $\alpha^*_{E,23}$ and $\alpha^*_{E,32}$.

spherical symmetry, we only focus on $\alpha^*_{E,11}$ in the following discussion.

Figure 2 shows the ME voltage coefficient $\alpha^*_{E,11}$ with respect to the crystallographic orientation of CFO and LNO. We observe that the maximum of -2.6711 V cm^{-1} Oe^{-1} occurs at Euler angles $(\alpha_i, \beta_i, \gamma_i) = (\alpha, 0, \gamma)$ and $(\alpha_m, \beta_m, \gamma_m) = (30°, 38°, 90°)$, where α and γ are arbitrary. Here the subscripts i and m denote the inclusion and matrix, respectively. The degeneracy of the optimal orientation $(\alpha_i, \beta_i, \gamma_i)$ reflects the 6 mm symmetry. Further, if $\alpha = 0$ and $\gamma = 0$, it is equivalent to the magnetic axis along [001]. The optimized value of -2.6711 V cm^{-1} Oe^{-1} is almost 1.27 times higher than -2.1023 V cm^{-1} Oe^{-1}, which is the value of the normal cut where the c axis of the CFO and LNO is along the x_3-axis.

Figure 3(a) shows the effect of the volume fraction f on the ME voltage coefficient. The PE phase is poled along the optimized direction $(\alpha_m, \beta_m, \gamma_m) = (30°, 38°, 90°)$ and the PM phase is along one of the optimized magnetic axes, say [001]. The maximum value is obtained at a volume fraction of $f = 0.92$ for the ME voltage coefficient $\alpha^*_{E,11}$. Therefore, the maximum value of $\alpha^*_{E,11}$ is -2.6711 V cm^{-1} Oe^{-1}.

Further, we observe that there are off-diagonal elements $\alpha^*_{E,23}$ and $\alpha^*_{E,32}$ when the poling direction/magnetic axis are in the optimal orientation. Figure 3(b) shows how these coefficients depend on the volume fraction. Remarkably, the maximum $\alpha^*_{E,23}$ is 19.6225 V cm^{-1} Oe^{-1}, while that of $\alpha^*_{E,32}$ is -10.8744 V cm^{-1} Oe^{-1}. Both of them occur when the PM particles almost completely fill the matrix ($f = 0.99$).

Finally, we replace the PE material by barium titanate ($BaTiO_3$, BTO) which is uniaxial (i.e. 6 mm symmetry). The maximum ME voltage coefficient $\alpha^*_{E,11}$ is -1.9645 V cm^{-1} Oe^{-1} at a volume fraction of $f = 0.98$ (figure 4). Now, the optimal orientation is also on the normal cut (i.e. c axis out of plane) (figure 5).

4.2. Piezoelectric particles in a piezomagnetic matrix

We now turn to the composite made of LNO particles in a CFO matrix. Similarly, we begin with the case of the material symmetry about the x_3 -axis, i.e. along [001]. The maximum

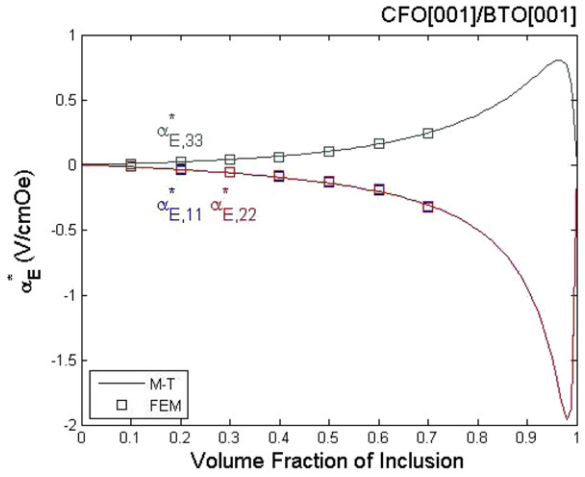

Figure 4. The ME voltage coefficients of the CFO particles in a BTO matrix in the normal direction versus the particle volume fraction.

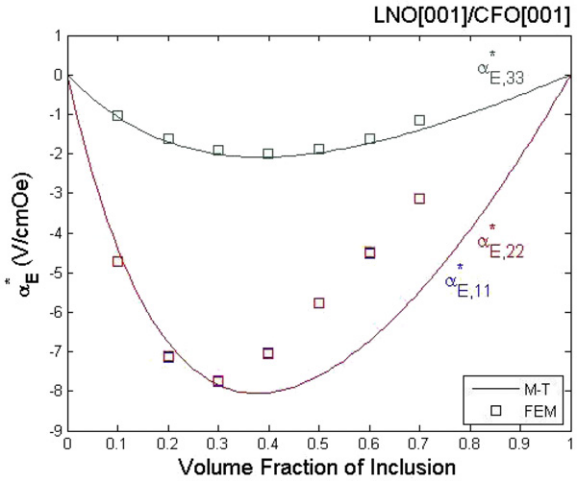

Figure 6. The ME voltage coefficients of the LNO particles in a CFO matrix in the normal direction versus the particle volume fraction.

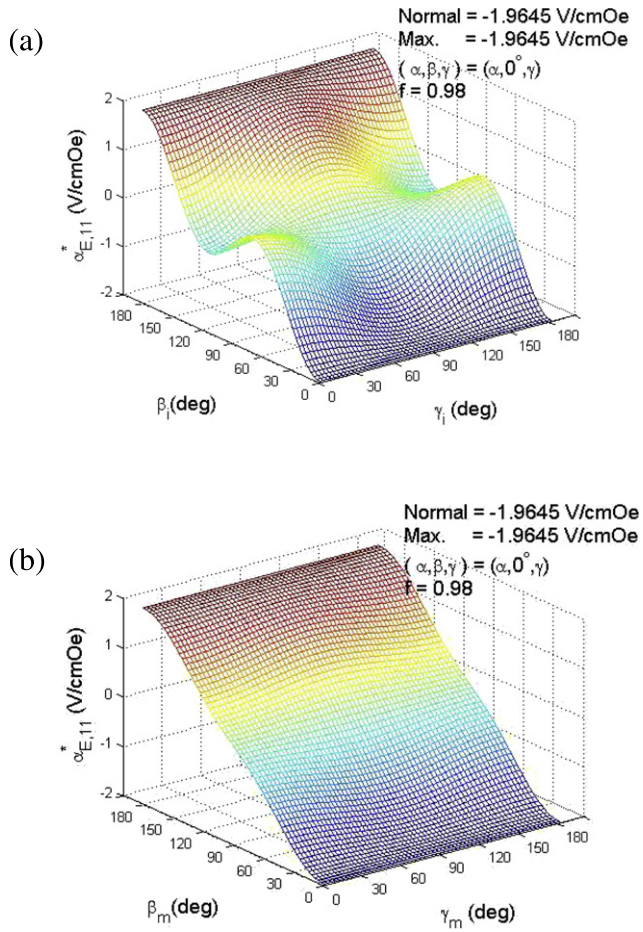

Figure 5. The ME voltage coefficient $\alpha^*_{E,11}$ of the CFO particles in a BTO matrix for various orientations of the CFO and BTO. The optimized constant occurs for both phases poled along the same direction. Note that this coefficient is independent of the Euler angles α_i and α_m.

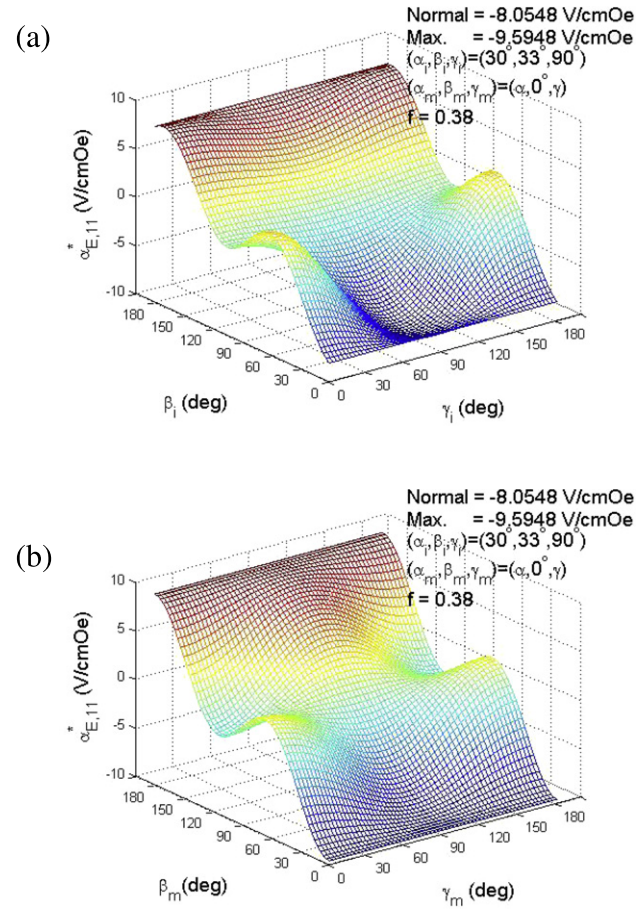

Figure 7. The ME voltage coefficient $\alpha^*_{E,11}$ of the LNO particles in a CFO matrix for various orientations of the LNO and CFO. The subscripts i and m denote the inclusion and matrix, respectively. Note that this coefficient is independent of the Euler angle α_m.

$\alpha^*_{E,11}$ and $\alpha^*_{E,22}$ are -8.0548 V cm^{-1} Oe^{-1} at $f = 0.38$, while $\alpha^*_{E,33}$ is -2.0829 V cm^{-1} Oe^{-1} at $f = 0.39$ in their normal orientation (figure 6).

Figure 7 shows the ME voltage coefficient $\alpha^*_{E,11}$ as a function of orientation for the case where the volume fraction corresponds to the optimal value at the normal

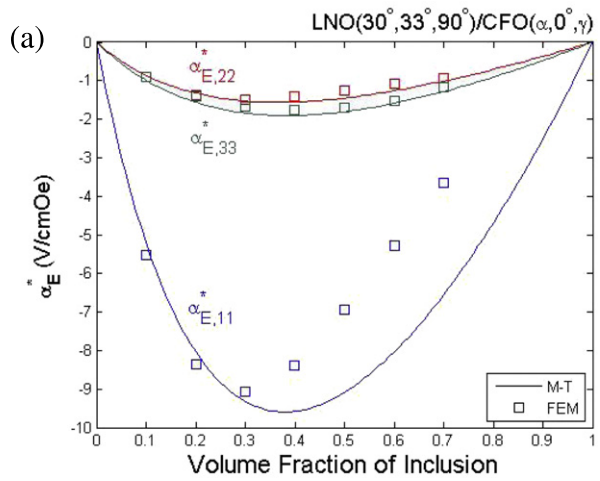

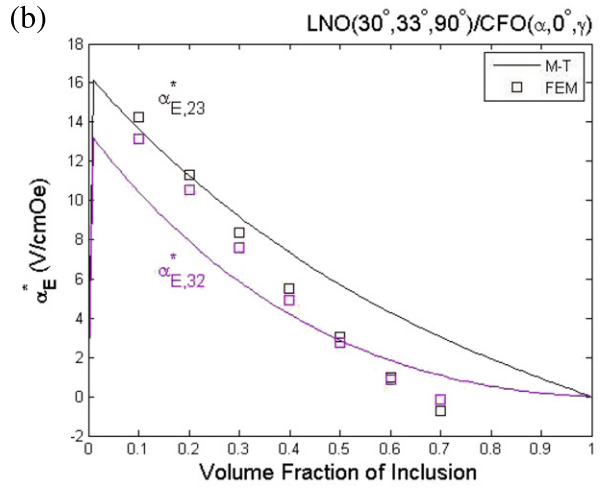

Figure 8. The optimal ME voltage coefficients of the LNO particles in a CFO matrix for various particle volume fractions. (a) Diagonal ME voltage coefficients $\alpha^*_{E,11}$, $\alpha^*_{E,22}$ and $\alpha^*_{E,33}$. (b) Off-diagonal ME voltage coefficients $\alpha^*_{E,23}$ and $\alpha^*_{E,32}$.

cut. We find that the maximum coupling coefficient is -9.5948 V cm^{-1} Oe^{-1} with $(\alpha_i, \beta_i, \gamma_i) = (30°, 33°, 90°)$ and $(\alpha_m, \beta_m, \gamma_m) = (\alpha, 0, \gamma)$, where α and γ are arbitrary. The enhancement is 19%. If we choose $\alpha = 0$ and $\gamma = 0$, the optimized direction is equivalent to [001].

Figure 8(a) shows the effect of the particle volume fraction on the ME voltage coefficient. For the optimized volume fraction, the value is -9.5948 V cm^{-1} Oe^{-1} ($f = 0.38$). This is evaluated for its optimal orientation.

Similarly, we observe that there are off-diagonal elements $\alpha^*_{E,23}$ and $\alpha^*_{E,32}$ when the poling direction/magnetic axis are in the optimal orientation $(\alpha_i, \beta_i, \gamma_i) = (30°, 33°, 90°)$ and $(\alpha_m, \beta_m, \gamma_m) = (\alpha, 0, \gamma)$. Figure 8(b) shows how these coefficients depend on the volume fraction. The maximum $\alpha^*_{E,23}$ is 16.1127 V cm^{-1} Oe^{-1}, while that of $\alpha^*_{E,32}$ is 13.1806 V cm^{-1} Oe^{-1}. Both of them occur as the volume fraction approaches zero ($f = 0.01$).

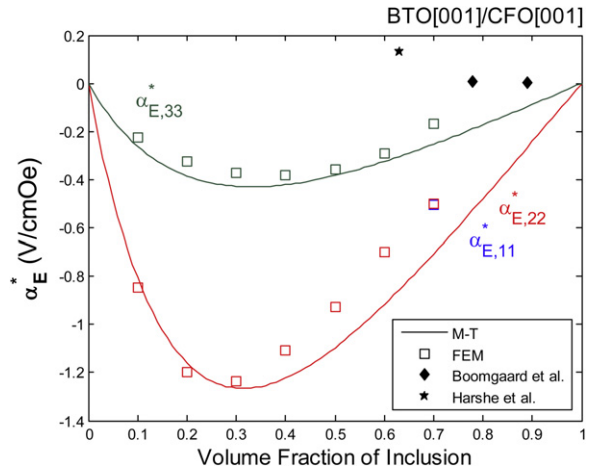

Figure 9. The ME voltage coefficients of the BTO particles in a CFO matrix in the normal direction versus the fiber volume fraction.

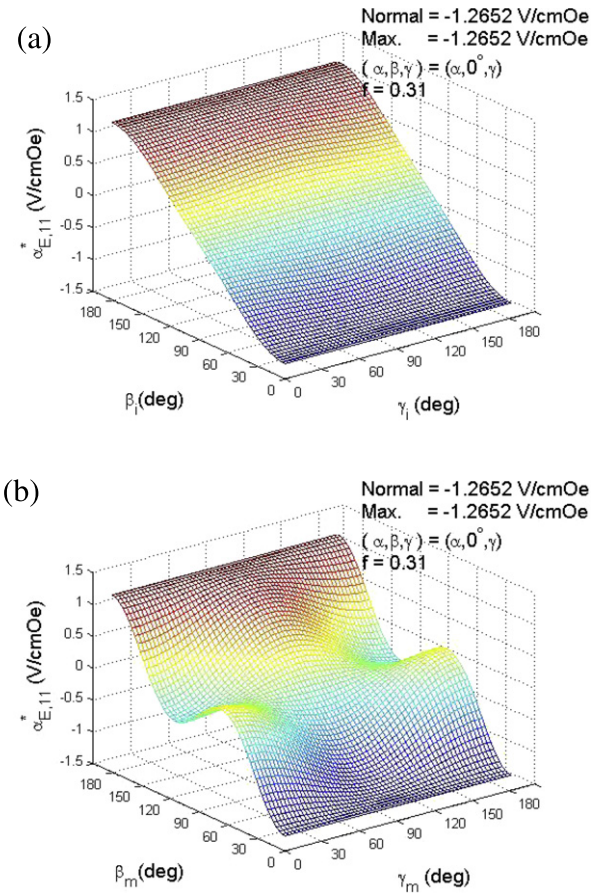

Figure 10. The ME voltage coefficient $\alpha^*_{E,11}$ of the BTO particles in a CFO matrix for various orientations of the BTO and CFO. The optimized constant occurs for both phases poled along the same direction. Note that this coefficient is independent of the Euler angles α_i and α_m.

Finally, we replace the PE material by barium titanate ($BaTiO_3$, BTO). The maximum ME voltage coefficient $\alpha^*_{E,11}$ is -1.2652 V cm^{-1} Oe^{-1} at a volume fraction of $f = 0.31$ (figure 9), and the optimal orientation is in this principal direction as well (figure 10).

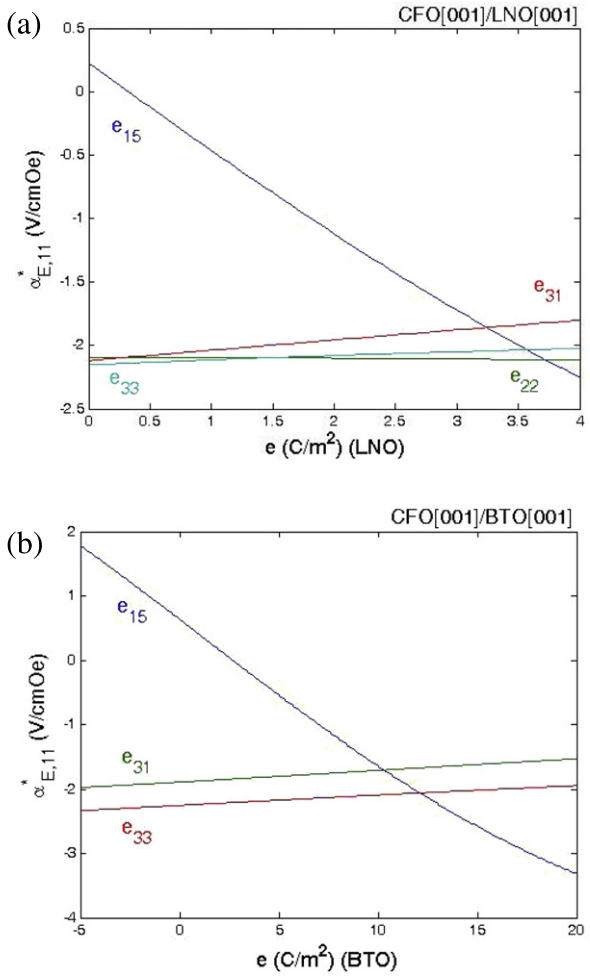

Figure 11. The ME voltage coefficient $\alpha^*_{E,11}$ versus the PE's piezoelectric coefficients. (a) CFO[0 0 1]/LNO[0 0 1], (b) CFO[0 0 1]/BTO[0 0 1].

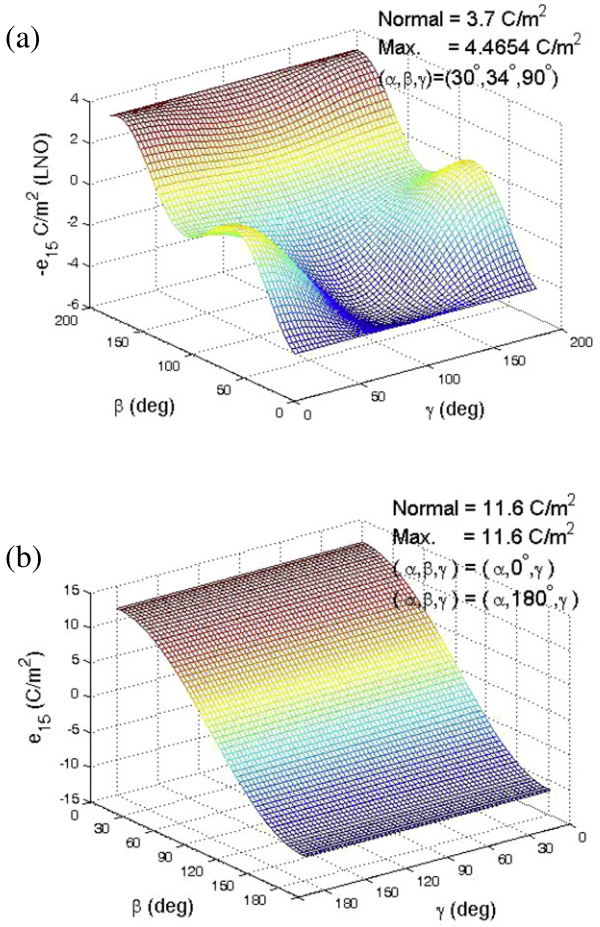

Figure 12. The piezoelectric constant e_{15} for various orientations of the PE phase. (a) LNO, (b) BTO.

Note that although the discrepancy between the Mori–Tanaka model and finite element method in figures 6 and 8(a), (b) and 9 is larger, the trend is similar for both methods. One reason for the deviation is that the ME voltage coefficient is an indirectly calculated value through equation (3.2). The effective permittivity κ^*_{ij} approaches zero and hence is sensitive when calculating $\alpha^*_{E,ij}$. Further, the ME coefficient λ^*_{ij} of these cases has a larger difference between the two approaches. This larger discrepancy was also observed by Lee *et al* (2005) for three-phase ME fibrous composites and by Kuo and Wang (2012) for ME fibrous composites with the poling direction not at the normal cut. For the sake of comparison with experiments and our theoretical results, the available data (van den Boomgaard *et al* 1976, Harshé *et al* 1993) for the ME voltage coefficient for the BTO–CFO composite are also shown in figure 9.

4.3. Relations between the ME voltage coefficient and the piezoelectric constant

From the above numerical results, we observe that when the PE phase is LNO, we can enhance the ME effect by rotating the poling direction. However, if the PE phase is BTO, the optimal orientation is in its principal direction. Therefore, we cannot improve the coupling through the crystal anisotropy for the latter case. Motivated by this observation, we study the relations between the ME voltage coefficient and the piezoelectric constant in this subsection.

We first study how the ME voltage coefficient $\alpha^*_{E,11}$ depends on the piezoelectric coefficient of the PE phase in figure 11. It is observed that among all the components of the piezoelectric coefficients e_{ij}, the constant e_{15} has a significant effect on the ME voltage coefficient for the above four cases, CFO/LNO, CFO/BTO, LNO/CFO and BTO/CFO. We take the two cases of CFO[0 0 1]/LNO[0 0 1] and CFO[0 0 1]/BTO[0 0 1] for example. If we assume $e_{15} = 0$ and all the remaining piezoelectric coefficients are equal to those of LNO or BTO, the ME voltage coefficient $\alpha^*_{E,11}$ of CFO/LNO decreases from -2.1023 V cm^{-1} Oe^{-1} to 0.2252 V cm^{-1} Oe^{-1} (figure 11(a)), while that of CFO/BTO decreases from -1.9645 V cm^{-1} Oe^{-1} to 0.6321 V cm^{-1} Oe^{-1} (figure 11(b)). Both are calculated at their optimal volume fractions. Similar results can be found for LNO/CFO and BTO/CFO. For the other piezoelectric components, they do not influence ME coupling much.

Next we plot the dependence between the LNO or BTO's e_{15} and its Euler angles β and γ in figure 12. It is interesting

that the contour has a similar trend with a dependence between the ME voltage coefficient $\alpha^*_{E,11}$ and the PE phase's Euler angles. For instance, the optimal orientation of LNO's e_{15} is at (30°, 34°, 90°) (figure 12(a)), which is close to the optimal orientation of CFO/LNO, (30°, 38°, 90°) (figure 2(b)), and LNO/CFO, (30°, 33°, 90°) (figure 7(a)). On the other hand, the optimal orientation of BTO's e_{15} is at its normal cut (figure 12(b)), which exactly corresponds to the optimal ME voltage constants of CFO/BTO (figure 5(b)) and BTO/CFO (figure 10(a)). Therefore, the piezoelectric constant e_{15} plays a major role in the determination of ME coupling for the ME particulate composite.

5. Conclusions

We have presented a micromechanical model for predicting the effective ME response of a spherical particulate composite of piezoelectric and piezomagnetic phases. The results are compared with finite element analysis. Both the magnitudes and the trends between them are in good agreement. For $CoFe_2O_4$–$LiNbO_3$ and $CoFe_2O_4$–$BaTiO_3$ particulate composites, the effects of crystallographic orientations and the volume fraction of the constituents on the ME voltage coefficients are investigated. For the CFO particles in an LNO matrix, the highest ME voltage coefficient $\alpha^*_{E,11}$ in its optimized crystallographic orientation is 2.6711 V cm^{-1} Oe^{-1}, which is 1.27 times larger than that of a particulate composite made with normal cut type CFO and LNO single crystals. For the LNO particles in a CFO matrix, the ME voltage coefficient $\alpha^*_{E,11}$ can be increased by around 1.19 times compared to the normal cut. For BTO–CFO particulate composites, however, the principal direction is their optimal direction. Finally, we have found that the ME voltage coefficient $\alpha^*_{E,11}$ is sensitive to the piezoelectric constant e_{15}, and the optimal orientation of the ME voltage coefficient $\alpha^*_{E,11}$ of the ME particulate composite is near that of the piezoelectric constant e_{15}.

Although various composites consisting of piezoelectric and magnetic oxide ceramics have been investigated experimentally in the past decades, at least to the best of the authors' knowledge, there is no well-known experimental result for optimum crystallographic orientations of ME particulate composites. We believe that this framework will stimulate new experimental works on ME coupling of anisotropic heterogeneous media, and be beneficial as design tools for engineering magnetoelectric composites.

Acknowledgment

We are grateful for the financial support of the National Science Council, Taiwan, under contract No. NSC 100-2628-E-009-022-MY2.

References

Aboudi J 2001 Micromechanical analysis of fully coupled electro–magneto–thermo–elastic multiphase composites *Smart Mater. Struct.* **10** 867–77

Alshits V I, Darinskii A N and Lothe J 1992 On the existence of surface waves in half-infnite anisotropic elastic media with piezoelectric and piezomagnetic properties *Wave Motion* **16** 265–84

Arfken G B and Weber H J 2001 *Mathematical Methods for Physicists* (San Diago: Academic) p 199

Astrov D N 1960 The magnetoelectric effect in antiferromagnetics *Sov. Phys.—JETP* **11** 708–9

Bayrashev A, Robbins W P and Ziaie B 2004 Low frequency wireless powering of microsystems using piezoelectric–magnetostrictive laminate composites *Sensors Actuators* **114** 244–9

Benveniste Y 1995 Mangetoelectric effect in fibrous composites with piezoelectric and piezomagnetic phases *Phys. Rev.* B **51** 16424–7

Bichurin M I, Petrov V M, Averkin S V and Liverts E 2010 Present status of theoretical modeling the magnetoelectric effect in magnetostrictive–pizoelectric nanostructures. Part I.: low frequency electromechanical resonance ranges *J. Appl. Phys.* **107** 053904

Bichurin M I, Petrov V M and Srinivasan G 2003 Theory of low-frequency magnetoelectric coupling in magnetostrictive–piezoelectric bilayers *Phys. Rev.* B **68** 054402

Camacho-Montes H, Sabina F J, Bravo-Castillero J, Guinovart-Díaz R and Rodríguez-Ramos R 2009 Magnetoelectric coupling and cross-property connections in a square array of a binary composite *Int. J. Eng. Sci.* **47** 294–312

Catalan G and Scott J F 2009 Physics and applications of bismuth ferrite *Adv. Mater.* **21** 2463–85

Eerenstein W, Mathur N D and Scott J F 2006 Multiferroic and magnetoelectric materials *Nature* **442** 759–65

Fiebig M 2005 Revival of the magnetoelectric effect *J. Phys. D: Appl. Phys.* **38** R123–52

Harshé G, Dougherty J P and Newnham R E 1993 Theoretical modelling of 3-0/0-3 magnetoelectric composites *Int. J. Appl. Electromagn. Mater.* **4** 161–71

Huang J H and Kuo W-S 1997 The analysis of piezoelectric/piezomagnetic composite materials containing ellipsoidal inclusions *J. Appl. Phys.* **81** 1378–86

Kim J-Y 2011 Micromechanical analysis of effective properties of magneto-electro-thermo-elastic multilayer composites *Int. J. Eng. Sci.* **49** 1001–18

Kittel C 2005 *Introduction to Solid State Physics* (New Jersey: Wiley) p 8

Kuo H-Y 2011 Multicoated elliptic fibrous composites of piezoelectric and piezomagnetic phases *Int. J. Eng. Sci.* **49** 561–75

Kuo H-Y and Pan E 2011 Effective magnetoelectric effect in multicoated circular fibrous multiferroic composites *J. Appl. Phys.* **109** 104901

Kuo H-Y, Slinger A and Bhattacharya K 2010 Optimization of magnetoelectricity in piezoelectric–magnetostrictive bilayers *Smart Mater. Struct.* **19** 125010

Kuo H-Y and Wang Y-L 2012 Optimization of magnetoelectricity in multiferroic fibrous composites *Mech. Mater.* **50** 88–99

Lee J, Boyd J G IV and Lagoudas D C 2005 Effective properties of three-phase electro-magneto-elastic composites *Int. J. Eng. Sci.* **43** 790–825

Li J Y 2000 Magnetoelectroelastic multi-inclusion and inhomogeneity problems and their applications in composite materials *Int. J. Eng. Sci.* **38** 1993–2001

Li J Y and Dunn M L 1998a Micromechanics of magnetoelectroelastic composite materials: average fields and effective behaviour *J. Intell. Mater. Syst. Struct.* **9** 404–16

Li J Y and Dunn M L 1998b Anisotropic coupled-field inclusion and inhomogeneity problems *Phil. Mag.* A **77** 1341–50

Liu G, Nan C-W, Cai N and Lin Y 2004 Calculations of giant magnetoelectric effect in multiferroic composites of rare-earth–iron alloys and PZT by finite element method *Int. J. Solids Struct.* **41** 4423–34

Lottermoser T, Lonkai T, Amann U, Hohlwein D, Ihringer J and Fiebig M 2004 Magnetic phase control by an electric field *Nature* **430** 541–4

Nan C-W 1994 Magnetoelectric effect in composites of piezoelectric and piezomagnetic phases *Phys. Rev.* B **50** 6082–8

Nan C-W, Bichurin M I, Dong S, Viehland D and Srinivasan G 2008 Multiferroic magnetoelectric composites: historical perspective, status, and future directions *J. Appl. Phys.* **103** 031101

Nye J F 1985 *Physical Properties of Crystals* (Oxford: Oxford University Press)

Pan E 2001 Exact solution for simply supported and multilayered magneto-electro-elastic plates *J. Appl. Mech.* **68** 608–18

Rado G T and Folen V J 1961 Observation of the magnetically induced magnetoelectric effect and evidence for antiferromagnetic domains *Phys. Rev. Lett.* **7** 310–1

Ramesh R and Spaldin N A 2007 Multiferroics: progress and prospects in thin films *Nature Mater.* **6** 21–9

Srinivas S, Li J Y, Zhou Y C and Soh A K 2006 The effective magnetoelectroelastic moduli of matrix-based multiferroic composites *J. Appl. Phys.* **99** 043905

Srinivasan G, Rasmussen E T, Galleogos J, Srinivasan R, Bokhan Y I and Laletin V M 2001 Magnetoelectric bilayer and multilayer structures of magnetostrictive and piezoelectric oxides *Phys. Rev.* B **64** 214408

Tang T and Yu W 2008 Variational asymptotic homogenization of heterogeneous electromagnetoelastic materials *Int. J. Eng. Sci.* **46** 741–57

Tang T and Yu W 2009 Micromechanical modeling of the multiphysical behavior of smart materials using the variational asymptotic method *Smart Mater. Struct.* **18** 125026

van den Boomgaard J, van Run A M J G and van Suchtelen J 1976 Magnetoelectricity in piezoelectric–magnetostrictive composites *Ferroelectrics* **10** 295–8

Vopsaroiu M, Blackburn J and Cain M G 2007 A new magnetic recording read head technology based on the magneto-electric effect *J. Phys. D: Appl. Phys.* **40** 5027–33

Wang J *et al* 2003 Epitaxial $BiFeO_3$ multiferroic thin film heterostructures *Science* **299** 1719–22

Wang Y, Or S W, Chan H L W, Zhao X and Luo H 2008 Enhanced magnetoelectric effect in longitudinal–transverse mode Terfenol-D/Pb($Mg_{1/3}Nb_{2/3}$)O_3-$PbTiO_3$ laminate composites with optimal crystal cut *J. Appl. Phys.* **103** 124511

Weis R S and Gaylord T K 1985 Lithium niobate: summary of physical properties and crystal structure *Appl. Phys.* A **37** 191–203

Yang P, Zhao K, Yin Y, Wan H G and Shu J S 2006 Magnetoelectric effect in magnetostrictive/piezoelectric laminate composite Terfenol-D/$LiNbO_3$[(zxtw)129°/30°] *Appl. Phys. Lett.* **88** 172903